

Martijn M. de Ruiter, Chris I. De Zeeuw and Christian Hansel

J Neurophysiol 96:378-390, 2006. First published Apr 5, 2006; doi:10.1152/jn.00906.2005

You might find this additional information useful...

This article cites 49 articles, 21 of which you can access free at:

<http://jn.physiology.org/cgi/content/full/96/1/378#BIBL>

This article has been cited by 2 other HighWire hosted articles:

Synaptic Plasticity and Calcium Signaling in Purkinje Cells of the Central Cerebellar Lobes of Mormyrid Fish

V. Z. Han, Y. Zhang, C. C. Bell and C. Hansel

J. Neurosci., December 5, 2007; 27 (49): 13499-13512.

[\[Abstract\]](#) [\[Full Text\]](#) [\[PDF\]](#)

Physiology of Morphologically Identified Cells in the Posterior Caudal Lobe of the Mormyrid Cerebellum

Y. Zhang and V. Z. Han

J Neurophysiol, September 1, 2007; 98 (3): 1297-1308.

[\[Abstract\]](#) [\[Full Text\]](#) [\[PDF\]](#)

Updated information and services including high-resolution figures, can be found at:

<http://jn.physiology.org/cgi/content/full/96/1/378>

Additional material and information about *Journal of Neurophysiology* can be found at:

<http://www.the-aps.org/publications/jn>

This information is current as of July 21, 2009 .

Voltage-Gated Sodium Channels in Cerebellar Purkinje Cells of Mormyrid Fish

Martijn M. de Ruiter, Chris I. De Zeeuw, and Christian Hansel

Department of Neuroscience, Erasmus University Medical Center, Rotterdam, The Netherlands

Submitted 30 August 2005; accepted in final form 31 March 2006

de Ruiter, Martijn M., Chris I. De Zeeuw, and Christian Hansel. Voltage-gated sodium channels in cerebellar Purkinje cells of mormyrid fish. *J Neurophysiol* 96: 378–390, 2006. First published April 5, 2006; doi:10.1152/jn.00906.2005. Cerebellar Purkinje cells of mormyrid fish differ in some morphological as well as physiological parameters from their counterparts in mammals. Morphologically, Purkinje cells of mormyrids have larger dendrites that are characterized by a lower degree of branching in the molecular layer. Physiologically, there are differences in electrophysiological response patterns that are related to sodium channel activity: first, sodium spikes in mormyrid Purkinje cells have low amplitudes, typically not exceeding 30 mV. Second, the response to climbing fiber stimulation in mormyrid Purkinje cells does not consist of a complex spike (with an initial fast sodium spike) as in mammals, but instead it consists of an all-or-none excitatory postsynaptic potential, the so-called climbing fiber response. Because of these unique properties, we have begun to characterize mormyrid Purkinje cells electrophysiologically. In this study, we provide a description of voltage-gated Na^+ channels and conductances in Purkinje cells of the mormyrid fish *Gnathonemus petersii*. Various types of Na^+ channel α -subunits, i.e., $\text{Na}_v1.1$, $\text{Na}_v1.2$, and $\text{Na}_v1.6$, have been described in rodent Purkinje cells. Using immunohistochemical techniques, we found that these subunits are present in Purkinje cells of mormyrids. To test whether these Na^+ channel subunits can mediate fast inactivating and resurgent Na^+ currents in *Gnathonemus* Purkinje cells, we conducted patch-clamp recordings in acutely dissociated cells and in cerebellar slices. Both types of Na^+ currents could be measured in rat and fish Purkinje cells. These data show that, despite prominent differences in electrophysiological response characteristics, Purkinje cells of rats and mormyrids share the same voltage-gated Na^+ conductances.

INTRODUCTION

The cerebellum of mormyrid fish has for quite some time attracted the attention of neuroanatomists because of its relative size (“gigantocerebellum”) and its unique organization (Meek 1992; Nieuwenhuys and Nicholson 1967, 1969). At the cellular level, a hallmark of the mormyrid cerebellum is the unusual architecture of the Purkinje cell dendritic tree, which differs substantially from that of mammalian Purkinje cells. Their dendrites show a palisade pattern displaying very different branching characteristics. The smooth proximal dendrites do not protrude into the molecular layer and run parallel to the boundary between the ganglion cell layer (Purkinje cell layer in mammals) and the molecular layer. The proximal dendrites give rise to perpendicularly oriented dendrites, which mostly do not branch any further and run parallel to each other toward the cerebellar surface. The parallel fibers (PFs) selectively

contact these distal dendrites, whereas the climbing fiber (CF) input contacts the smooth proximal dendrite. This configuration leads to a far stronger spatial separation between PF and CF synapses than that known from mammalian Purkinje neurons. The axons of mormyrid Purkinje cells are very short. They project in the ganglion cell layer itself onto efferent cells (also called eurydendroid cells) and neighboring Purkinje cells. The efferent cells represent a functional equivalent to the cerebellar nuclei neurons in mammals and provide the sole output of the mormyrid cerebellum (Meek 1992; Meek and Nieuwenhuys 1991; Nieuwenhuys and Nicholson 1967, 1969).

The unusual dendritic tree architecture and synaptic input organization of mormyrid Purkinje cells motivated us to attempt to characterize these cells electrophysiologically. Although the medium ganglion cells (Purkinje-like interneurons) in the mormyrid electrosensory lobe (a cerebellum-like structure) have been characterized with regard to several electrophysiological parameters and with regard to synaptic plasticity (e.g., Bell et al. 1997a,b; Han et al. 2000), the physiological description of cerebellar Purkinje cells of mormyrid fish has only recently begun (Han and Bell 2003). Our initial recordings focused on synaptic responses of mormyrid Purkinje cells to CF stimulation. In mammalian Purkinje cells, CF activation results in a large all-or-none response, the so-called complex spike, which consists of an initial, fast spike component followed by a series of smaller spikelets riding on top of a plateau (for review see Schmolesky et al. 2002). The fast, initial spike is generated by a somatic Na^+ current. The following slower components were described as resulting from the activation of dendritic Ca^{2+} conductances (Llinas and Sugimori 1980a,b). More recently, it was shown that complex spike-like events can be evoked in the soma by intromatic depolarization or anode break stimulation (Callaway and Ross 1997) and can even be elicited in dissociated Purkinje cells (Swensen and Bean 2003). Thus it is likely that the complex spike is triggered by dendritic events, but that, at least at the somatic level, the slow complex spike components are mediated by somatic Na^+ and Ca^{2+} currents (for discussion see Schmolesky et al. 2002), which can be activated locally.

In contrast to mammals, stimulation of the CF in the cerebellum of the mormyrid fish *Gnathonemus petersii* does not elicit a complex spike, but rather an all-or-none “CF response” that lacks obvious spike components (see following text). These CF responses can occur in isolation, but they are often followed by series of “small spikes” shown to be Na^+ spikes, probably originating from the axon, reaching amplitudes of

Address for reprint requests and other correspondence: C. Hansel, Department of Neuroscience, Erasmus University Medical Center, P.O. Box 1738, 3000 DR Rotterdam, The Netherlands (E-mail: c.hansel@erasmusmc.nl).

The costs of publication of this article were defrayed in part by the payment of page charges. The article must therefore be hereby marked “advertisement” in accordance with 18 U.S.C. Section 1734 solely to indicate this fact.

≤30 mV (Han and Bell 2003). The absence of otherwise Purkinje cell-typical complex spikes and the presence of small-amplitude Na⁺ spikes, which have not been described in other types of neurons, are the most obvious electrophysiological features that distinguish mormyrid Purkinje cells from their mammalian counterparts. Both the unique morphological and electrophysiological properties motivated us to attempt to characterize mormyrid Purkinje cells in more detail.

Voltage-gated Na⁺ channels consist of an α -subunit and one or more β -subunits. The α -subunit forms the channel pore and possesses all the main properties of the channel such as voltage-dependent gating and Na⁺ selectivity. The β -subunits are capable of changing the channel kinetics as well as the voltage dependency of inactivation (Isom et al. 1995a,b). In the adult mammalian cerebellum, three types of Na⁺ channel α -subunits are expressed: α Na_v1.1, α Na_v1.2, and α Na_v1.6 (equivalent to rat brain I, rat brain II, and Scn8a; Gong et al. 1999; Vega-Saenz de Miera et al. 1997; Westenbroek et al. 1989). Na⁺ channel α -subunits of teleost fish, the taxonomical group to which mormyrid fish belong, show high homology to Na⁺ channel α -subunits of rats. Goldfish α Na_v1.2 and α Na_v1.6 subunits, for instance, show 77 and 87% homology with α Na_v1.2 and α Na_v1.6 subunits in rats (Zenisek et al. 2001). In addition, two β -subunits (β 1, β 2) are expressed. The different subunits are heterogeneously distributed in different cell types (for review see Schaller and Caldwell 2003). Mammalian Purkinje cells express Na⁺ channel α -subunits Na_v1.1 and Na_v1.6 in both soma and dendrites (Gong et al. 1999; Schaller and Caldwell 2003). Reports on the expression of Na_v1.2 in Purkinje cells are conflicting (Black et al. 1994; Felts et al. 1997; but see Brysch et al. 1991; Gong et al. 1999).

Electrophysiologically, three tetrodotoxin (TTX)-sensitive Na⁺ conductances were described in mammalian cerebellar Purkinje cells. Recordings from Purkinje cells in slices or organotypic cultures revealed a fast inactivating and a persistent Na⁺ conductance (Gähwiler and Llano 1989; Kay et al. 1998; Llinas and Sugimori 1980a). Additionally, Raman and Bean described a third Na⁺ current mediated by Na_v1.6 channels, the “resurgent Na⁺ current” (Raman and Bean 1997, 2001; Raman et al. 1997), which can be elicited on repolarization after a depolarization to positive potentials. There are uncertainties about the assignment of the different subunit types to particular currents. Recordings from Purkinje cells of Na_v1.6 knockout mice indicate that Na_v1.6 channels mediate large parts of the resurgent Na⁺ current (Raman et al. 1997). The fast, inactivating Na⁺ currents and the persistent Na⁺ currents were reduced in those mutant mice as well, but to a lower degree. These observations indicate that Na_v1.6 channels participate in all three types of currents, but that Na_v1.1 and Na_v1.2 channels are involved in the fast, inactivating Na⁺ currents and/or the persistent Na⁺ currents as well (for discussion see Kay et al. 1998; Schaller and Caldwell 2003).

Na_v1.6-mediated resurgent Na⁺ currents are pleomorphic in nature. Whereas in Na_v1.6 null mutant mice resurgent currents are normally absent or very small in Purkinje cells (Grieco and Raman 2004), subthalamic nucleus neurons from Na_v1.6-null mutants show considerable resurgent Na⁺ currents (37% of wild type) (Do and Bean 2004). Another example illustrating the pleomorphic nature is provided by CA3 pyramidal neurons and motor neurons, which do express Na_v1.6 Na⁺ channels but lack resurgent Na⁺ currents (Garcia et al. 1998; Pan and Bean

1999; Raman and Bean 1997). Resurgent Na⁺ currents mediated by Na_v1.6 channels can recover from inactivation at relatively depolarized potentials (Khaliq et al. 2003; Raman and Bean 1997). This feature enables them to accelerate spike firing during bursts. It is therefore likely that resurgent Na⁺ currents also contribute to the late complex spike components, which can reach frequencies >200 Hz. Although there are still gaps in our understanding of which conductances are mediated by which types of Na⁺ channel α -subunits, it can be shown that alterations in the expression pattern of Na⁺ channel α -subunits lead to changes in the firing pattern of Purkinje cells. For example, Purkinje cells from mice lacking Na_v1.6 channels show not only a reduction in resurgent currents, but also diminished repetitive spike firing (Raman et al. 1997). Biolistic introduction of Na_v1.8 cDNA into Purkinje cells reduced the number of spikes in conglomerate action potentials evoked by depolarizing current pulses (Renganathan et al. 2003), thus altering a characteristic feature of Purkinje cell electrophysiology. These observations emphasize that the expression profile of voltage-dependent Na⁺ channels provides an important component of a complete electrophysiological characterization of neurons, even if the expression of a certain type of subunit does not allow us to reliably predict associated conductances.

To characterize the functional expression of Na⁺ channel α -subunits, we applied immunohistochemistry to describe their distribution and performed voltage-clamp recordings to test for the presence of various types of voltage-gated Na⁺ conductances. All immunohistochemical as well as electrophysiological experiments were performed not only in Purkinje cells of the mormyrid fish *Gnathonemus petersii*, but also in rats to obtain reference values for comparison and to investigate the debated presence of Na_v1.2 Na⁺ channels in rat Purkinje cell membranes.

METHODS

Animals

Sprague–Dawley rats (Harlan Nederland, Horst, The Netherlands), aged P18–P28, were housed in filtertop cages. Mormyrid fish of the species *Gnathonemus petersii* (obtained from a local fish dealer) were wild caught and kept in standard aquaria. All experiments described were approved by the Erasmus Medical Center animal care and use committee.

Immunohistochemistry

Mormyrid fish and rats were anesthetized with 0.20 mmol/l eugenol and 0.2 ml Nembutal, respectively, and perfused with 4% paraformaldehyde in 0.02 M phosphate buffer (PB). Brains were removed, postfixed, and rinsed overnight at 4°C in 0.1 M PB, containing 10% sucrose. Embedding of the brains in gelatin was done as described by Groenewegen and Voogd (1977). Sections (40 μ m thick) were cut and collected in 0.1 M PB. Sections were rinsed in Tris-buffered saline (TBS) and preincubated for 1 h at 4°C in 10% normal horse serum (NHS) and 0.5% Triton in TBS.

Avidin–biotin complex (ABC) staining

Sections were incubated with primary antibody for 48 to 72 h at 4°C in incubation buffer 1 (IB1), containing 2% NHS and 0.4% Triton in TBS, and rinsed (TBS). Secondary antibody was added for 1.5 to 2 h at room temperature in IB1. Sections were rinsed again, after

which the biotin-labeled secondary antibody was conjugated with avidin from a Vectastain ABC kit (Vector Laboratories, Burlingame, CA). Sections were rinsed (TBS, Tris) and stained for 15 min using diaminobenzidine (DAB). Finally, sections were rinsed again (Tris, PB), put on slides, dried, and coverslipped.

Fluorescent labeling

Sections were incubated 48 h with primary antibody at 4°C in incubation buffer 2 (IB2), containing 1% NHS and 0.4% Triton in TBS, and rinsed (TBS). Sections were then incubated for 90 min with secondary antibody in IB2 and rinsed (TBS). Finally, they were mounted on slides and coverslipped.

Primary antibodies used were: rabbit anti-brain type I Na⁺ channel (Na_v1.1) directed against peptide (KY)TAS EHSRE PSAAG RLSG, corresponding to residues 465–481 of rat Na_v1.1 intracellular loop between domains I and II (accession P04774); rabbit anti-Na_v1.2 directed against peptide (KY)ASA ESRDF SGAGG IGVFS E, corresponding to residues 467–485 of rat Na_v1.2 intracellular loop between domains I and II (accession P04775); rabbit anti-Scn8a (Na_v1.6) directed against peptide CIANH TGVDI HRNGD FQKNG, corresponding to residues 1042–1061 of rat Scn8a intracellular loop between domains II and III (accession AAC26014) (Alomone Labs, Jerusalem, Israel); and rabbit anti-inositol 1,4,5-trisphosphate (IP₃)-receptor subtype I (Calbiochem, Amsterdam, The Netherlands). Secondary antibodies used were: biotinylated goat anti-rabbit (Bio-Gar; Vector Laboratories) and fluorescein-isothiocyanate (FITC)-labeled donkey anti-rabbit (FITC-Dar; Jackson Labs, Amsterdam, The Netherlands). All other drugs were purchased from Sigma.

Control experiments for antibody staining

The specificity of the immunohistochemical procedure was examined by performing parallel incubations in which the primary antibody was omitted or preadsorbed. Before preadsorption testing we first determined the antibody concentration at which staining was just visible. For all three Na⁺ channel primary antibodies used this concentration was 1:100. We then doubled the primary antibody concentration and 1 h before incubating the sections, as suggested by Saper and Sawchenko (2003), we added 50 μM/ml of antigen against which the primary antibody was raised. We used three different control antigens (rat) for the three Na⁺ channel primary antibodies (Alomone Labs).

Western blots

Rats and mormyrid fish were anesthetized with halothane or 0.20 mmol/l eugenol, respectively, and decapitated; brains were removed and put on ice in 320 mM sucrose with protease inhibitor cocktail (Boehringer-Mannheim). Brains were homogenized and centrifuged at 2,000 × *g* for 5 min. Supernatant was collected and centrifuged at 100,000 × *g* for 1 h at 4°C after which the pellet was resuspended in 320 mM sucrose with protease inhibitor cocktail to a final concentration of 2,000 μg per 10 μl and stored at –80°C. Samples were mixed with sample buffer and samples plus markers (Biorad) were heated for 10 min at 70°C; 10 μl of sample per lane was applied to a 7% polyacrylamide gel. Gels were run for 1.5 h at 30 mA/gel under standard conditions. After running the gel was completed and proteins were transferred onto a nitrocellulose membrane for 1.5 h using standard wet-blot techniques at 100 mA per gel. Blots were then blocked with 5% nonfat dry milk in PBS and 0.025% Na-azide for 2 h at room temperature. Blots were incubated with primary antibody (anti-Na_v1.1, 1.2, and 1.6, final concentration 1:100; Alomone Labs) for 2 h at room temperature in blocking solution. Blots were then washed four times for 10 min with PBS containing 0.1% Tween 20. Incubation with secondary antibody [SwaR-HRP (swine anti-rabbit conjugated with horseradish peroxidase) 1:4,000; Dako, Glostrup,

Denmark] was done at room temperature for 1 h. After the blot was washed again ECL was performed using a commercial kit (Amersham Bioscience). Film (Kodak) was developed on a Kodak film processor.

Photography

Photographs (Fig. 2, *A* and *B* and Figs. 3, 4, and 5, panels *A–F*) were taken using a digital camera (Leica) mounted on a brightfield microscope (Leica). Brightness and contrast were enhanced to comparable levels using the camera's software package (Leica) and microscope settings before the pictures were taken. Fluorescent images (Fig. 2, *C* and *D*) were taken using a confocal microscope (Zeiss). The image in Fig. 2*D* was constructed from a 15-image Z-stack using LSM photo software (Zeiss). Films developed for our Western blot experiments (Figs. 3*G*, 4*G*, and 5*G*) were scanned using an HP flatbed scanner.

Electrophysiology

The mormyrid cerebellum is subdivided into a valvula, a central corpus, and a caudal lobe (see Meek 1992). The corpus cerebelli consists of four central lobes, C1 to C4. Our recordings from mormyrid Purkinje cells were restricted to these central lobes. In the rat, all experiments were performed using the cerebellar vermis. All recordings were done at room temperature.

Slice recordings (Fig. 7): Rats and mormyrid fish were anesthetized with halothane or 0.20 mmol/l eugenol, respectively, and decapitated; brains were removed, cut into 200-μm-thick sagittal slices, and immersed in standard artificial cerebrospinal fluid (ACSF) containing (in mM): 124 NaCl, 5 KCl, 1.25 NaH₂PO₄, 26 NaHCO₃, 2 CaCl₂, 2 MgSO₄, and 10 D-glucose, bubbled with 95% O₂-5% CO₂. After a recovery period of ≥1 h, slices were placed in a submerged chamber and perfused at a flow rate of 1.6 ml/min with either bubbled ACSF (Fig. 1) or rACSF ("resurgent" artificial cerebrospinal fluid) containing (in mM): 122 NaCl, 5 TEA-Cl, 2 KCl, 1.25 NaH₂PO₄, 26 NaHCO₃, 2 CaCl₂, 2 MgSO₄, 10 D-glucose, and 0.30 CdCl₂ to block most Ca²⁺ and K⁺ currents (Figs. 6 and 7). Acutely dissociated cells (Fig. 6): Slices were prepared as mentioned. Rat cerebellar slices were then treated with 3 mg/ml protease XXIII in dissociation buffer (DB) containing (in mM): 82 Na₂SO₄, 30 K₂SO₄, 5 MgCl₂, 10 HEPES, and 10 glucose (buffered to pH 7.4 using NaOH) for 7 min at 37°C with oxygen blown over the surface. Tissue was washed in warm oxygenated DB containing 1 mg/ml BSA + 1 mg/ml trypsin inhibitor and was allowed to cool to room temperature. The tissue was then triturated in DB and maintained at room temperature with oxygen blown over the surface in Tyrode's solution containing (in mM): 150 NaCl, 4 KCl, 2 CaCl₂, 2MgCl₂, 10 HEPES, and 10 glucose (buffered to pH 7.4 using NaOH). Cells were used within 4 h after dissociation (Raman and Bean 1997). Fish slices were incubated for 15 min at room temperature using 40 U/ml Papain in Eagle's MEM incubation buffer (IB) containing (in mM): 10 HEPES, 1 cysteine, 0.5 EDTA, and 5 Na-acetate (pH 7.2). Slices were then washed and triturated in IB and kept in recording solution in the recording chamber to settle (Afshari et al. 2004). All recordings from acutely dissociated cells were made in rACSF. Recordings were performed using the visualized whole cell patch-clamp technique with a Zeiss Axioskop FS and an EPC-9 amplifier (HEKA Electronics, Lambrecht, Germany). Recording electrodes (resistance 3–5 MΩ) were filled with a solution containing (in mM): 9 KCl, 10 KOH, 120 K⁺-gluconate, 3.48 MgCl₂, 10 HEPES, 4 NaCl, 4 Na₂ATP, 0.4 Na₃GTP, and 17.5 sucrose (Fig. 1, *A–C*) or (in mM): 128 CsOH, 111 gluconic acid, 4 NaOH, 10 CsCl, 2 MgCl₂, 10 HEPES, 4 Na₂ATP, 0.4 Na₃GTP, and 30 sucrose (Figs. 1, *D–F*, 6, and 7; Hansel and Linden 2000). Both types of internal saline were pH-adjusted (pH 7.25).

Currents were filtered at 3 kHz and digitized at 8 kHz using Pulse software. For extracellular stimulation (Fig. 1), standard patch pipettes were filled with external saline. Climbing fibers were stimulated in the

granule cell layer. Voltage-step protocols used were either: a 20-ms depolarizing step from -90 to +30 mV followed by repolarizing steps to potentials between 0 and -60 mV or a depolarizing ramp, 0.1 mV/ms from -90 to +30 mV followed by repolarizing steps between +20 and -60 mV (Raman and Bean 1997). Traces recorded in rACSF containing 300 nM TTX were subtracted from traces recorded in rACSF alone to isolate TTX-sensitive Na⁺ currents from, e.g., capacitive and leak currents (Figs. 6 and 7). Directly after forming a gigaseal the fast capacitance was corrected using the automatic capacitance compensation function embedded in the amplifier window of the HEKA Pulse software package. After break-in (whole cell configuration) the slow capacitance was compensated the same way. All drugs were purchased from Sigma.

RESULTS

Synaptic responses to CF stimulation

In mammalian Purkinje cells, CF activation results in the firing of a complex spike. Figure 1A shows a complex spike recorded from a rat Purkinje cell. The complex spike is characterized by an initial somatic Na⁺ spike, followed by a slow plateau potential with small spikelets on top. The plateau potential could result from Ca²⁺ currents and/or noninactivating Na⁺ currents in the Purkinje cell soma and proximal dendrites (Llinas and Sugimori 1980a,b; for review see Schmolesky et al. 2002). The origin of the small spikelets is still not resolved. Although the complex spike is initiated by

the activation of dendritic α -amino-3-hydroxy-5-methyl-4-isoxazolepropionic acid (AMPA) receptors and subsequent local Ca²⁺ spike activity, it is likely that the spikelets, as recorded in the soma, are mediated by somatic Ca²⁺ and Na⁺ currents. Resurgent Na⁺ currents might facilitate the high-frequency discharge that characterizes the late complex spike components. The climbing fiber response of mormyrid fish (*Gnathonemus petersii*) differs substantially from its mammalian counterpart in several aspects (Fig. 1, B and C). The initial component is an all-or-none excitatory postsynaptic potential (EPSP; the all-or-none character is shown in Fig. 1B), which is sometimes followed by one or more small spikes that are thought to be axonal Na⁺ spikes that do not invade the soma (Han and Bell 2003). These small spikes may or may not occur (for examples of CF responses without and with small spikes see Fig. 1, B and C, respectively) and thus cannot be considered as a CF response component. CF-evoked excitatory postsynaptic currents (EPSCs) reverse typically around +12 mV in both rat and mormyrid fish Purkinje cells (Fig. 1, D and E). The amplitudes of mormyrid fish EPSCs are generally smaller than those recorded in rat Purkinje cells (Fig. 1, D and E). CF-EPSCs of both species show similar rise time kinetics when traces above and below the reversal potential were scaled to the same amplitude after the positive currents were reversed (Fig. 1F). Because voltage-gated Na⁺ channels are critically involved in the generation of complex spikes, and CF re-

Downloaded from jn.physiology.org on July 21, 2009

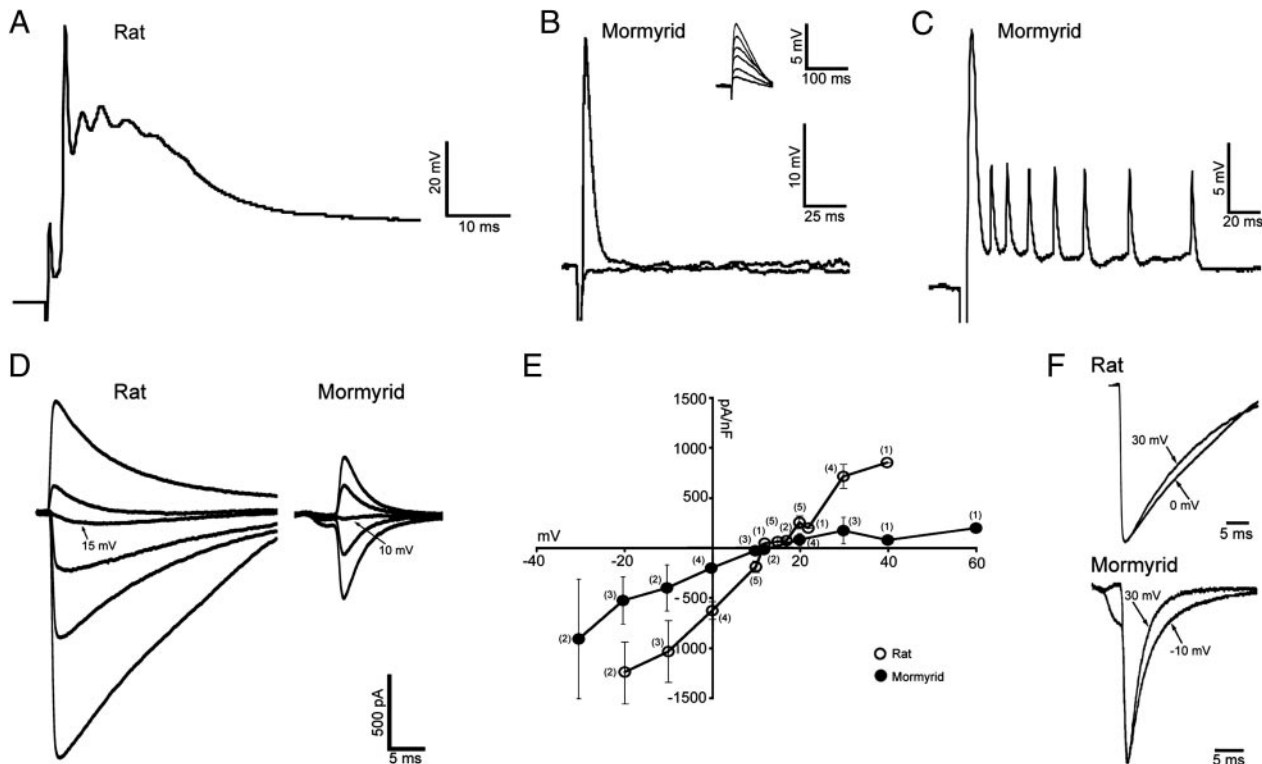


FIG. 1. Climbing fiber (CF)-evoked electrical responses in Purkinje cells. A: complex spike recorded from a rat Purkinje cell. B: all-or-none CF responses recorded from a *Gnathonemus petersii* Purkinje cell. Responses are shown above and below the threshold for evoking an excitatory postsynaptic potential (EPSP). Inset: series of parallel fiber EPSPs evoked at increasing stimulus intensities. Note the different timescales of the CF and parallel fiber (PF) response. C: example of a cell in which the EPSP was followed by small spikes. D: voltage dependency of CF EPSCs recorded from rat (left) and mormyrid Purkinje cells (right). Voltage steps (in mV) were +30, +20, +15, +10, 0, and -10 for the rat recording and +30, +20, +10, 0, and -10 for the fish recording. E: voltage dependency of CF-EPSCs measured in rat (n = 5) and fish Purkinje cells (n = 4). Not every voltage step was applied to every cell. Amplitudes are shown as means \pm SE. F: CF-EPSCs from D show comparable rising phase kinetics above and below the reversal potential (the positive currents were reversed and scaled to the same amplitude). Top: currents recorded from a rat Purkinje cell at +30 and 0 mV. Bottom: currents recorded from a fish Purkinje cell at +30 and -10 mV. Current amplitudes differ for the traces shown and amplitude scale bars were therefore omitted. Original traces are shown in D.

sponses differ substantially between rat and mormyrid fish, we wanted to determine the expression patterns of the three mammalian Na^+ channel α -subunits in mormyrid fish to better understand the molecular and cellular basis of the unique electrophysiological features of their Purkinje cells.

Immunohistochemistry

In mormyrid fish, cerebellar Purkinje cells can be confused with efferent cells or stellate cells, which have a roughly similar palisade pattern of their dendritic trees in the molecular layer. Reliable criteria for the identification of Purkinje cells are a particularly low degree of dendritic branching and the resulting regularity in appearance, the relative thickness of dendrites, the presence of dendritic spines, and the superficial position of the somata within the ganglion cell layer (Meek and Nieuwenhuys 1991). In addition, IP_3 -receptor subtype I is known to be selectively expressed in Purkinje cells (Koulen et al. 2000; Sharp et al. 1999). To obtain reference images for the identification of Purkinje cells, we used an antibody against the IP_3 -receptor subtype I. The DAB staining pattern for IP_3 -receptor subtype I was similar in both rat and mormyrid fish (Fig. 2, A and B). In rat sections, the Purkinje cells are easily identified by the unique shape of their dendritic trees. It is obvious from Fig. 2A that the staining was selective for Purkinje cells. In sections of mormyrid fish, the identity of the stained cells was confirmed by the presence of spines (Fig. 2D), which we could visualize using fluorescent secondary antibodies (Fig. 2, C and D). The presence of spines allows for an unambiguous identification of these cells as Purkinje cells because the other two types of neurons with palisade-shaped dendrites are aspiny (Meek 1992; Meek and Nieuwenhuys 1991). Thus in both rat and fish sections the staining for IP_3 -receptor subtype I was Purkinje cell specific.

To characterize the distribution pattern of $\text{Na}_v1.1$ channels, we immunostained cerebellar sections obtained from rats (Fig. 3, A and B) and from mormyrid fish (Fig. 3, C and D). In rat sections, Purkinje cell somata are stained and there is some staining in the molecular layer that, however, is too weak for identification of dendritic structures. In the fish sections, there is a staining of small and larger somata in the ganglion cell layer as well and also a similarly weak staining in the molecular layer. Figure 3, C and D shows pictures taken from the central lobe C2. In contrast to lobes 3 and 4, lobes 1 and 2 are known to have a layer of stellate cells external to the layer of Purkinje cells (VZ Han and CC Bell, personal communication). In Fig. 3D, smaller, more superficial somata can be distinguished from larger somata. Thus it is likely that somata of both stellate and Purkinje cells were stained. In contrast to the staining for $\text{Na}_v1.1$ channels, antibodies against $\text{Na}_v1.2$ channels led to a strong staining in rat Purkinje cells in both somata and dendrites (Fig. 4, A and B). Similarly, somata and dendrites of *Gnathonemus* Purkinje cells were heavily stained (Fig. 4, C and D). The dendrites could be clearly distinguished and the identification of Purkinje cells was based on the criteria as mentioned above.

A very similar staining pattern emerges from the antibody staining against $\text{Na}_v1.6$ channels. In rat sections, there is a strong staining in somata and dendrites of Purkinje cells (Fig. 5, A and B). A similar distribution can be seen in fish sections, where $\text{Na}_v1.6$ channels are also expressed in Purkinje cell somata and dendrites (Fig. 5, C and D). These results show that Purkinje cells in rats and mormyrid fish show the same expression pattern of Na^+ channel α -subunits. $\text{Na}_v1.1$ channels also appeared to be expressed in somata in the granule cell layer (these could be somata of Golgi cells, unipolar brush cells, or a subset of granule cells), whereas $\text{Na}_v1.2$ and 1.6 were found

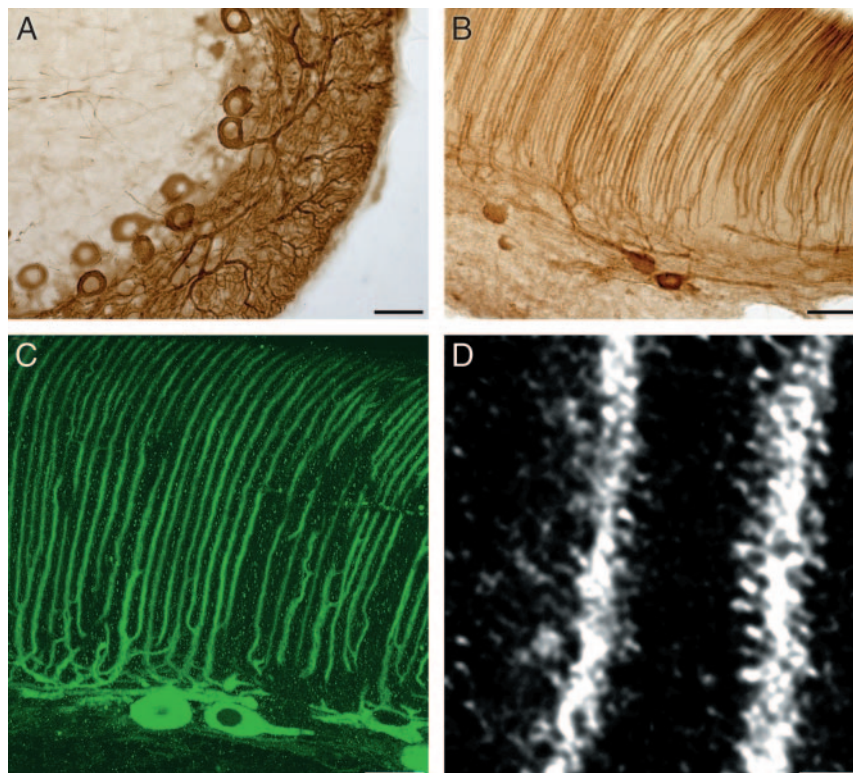


FIG. 2. Inositol 1,4,5-trisphosphate (IP_3)-receptor subtype I antibody staining. A: rat cerebellar section stained with anti- IP_3 -receptor subtype I antibodies and diaminobenzidine (DAB). Note the Purkinje cell specificity of the IP_3 -receptor in the cerebellum and the evenly dense staining in the somata and dendrites of the Purkinje cells. Top left: a few Purkinje cell axons are stained. B: staining as in A, but in a section of the mormyrid cerebellum. Note that the staining pattern of IP_3 -receptors is very similar between rat and fish (A and B), but that the architecture of the Purkinje cell dendrite is different. C: mormyrid cerebellar section stained with anti- IP_3 -receptor subtype I antibodies and fluorescein-isothiocyanate (FITC). Note that the dendrites of mormyrid Purkinje cells branch only a few times very proximally and then run straight to the pial surface. D: dendritic tree of a mormyrid Purkinje cell clearly shows numerous spines that are stained for IP_3 -receptors of subtype I (FITC). Scale bars = 12.5 μm in A and B, 20 μm in C, and 2 μm in D.

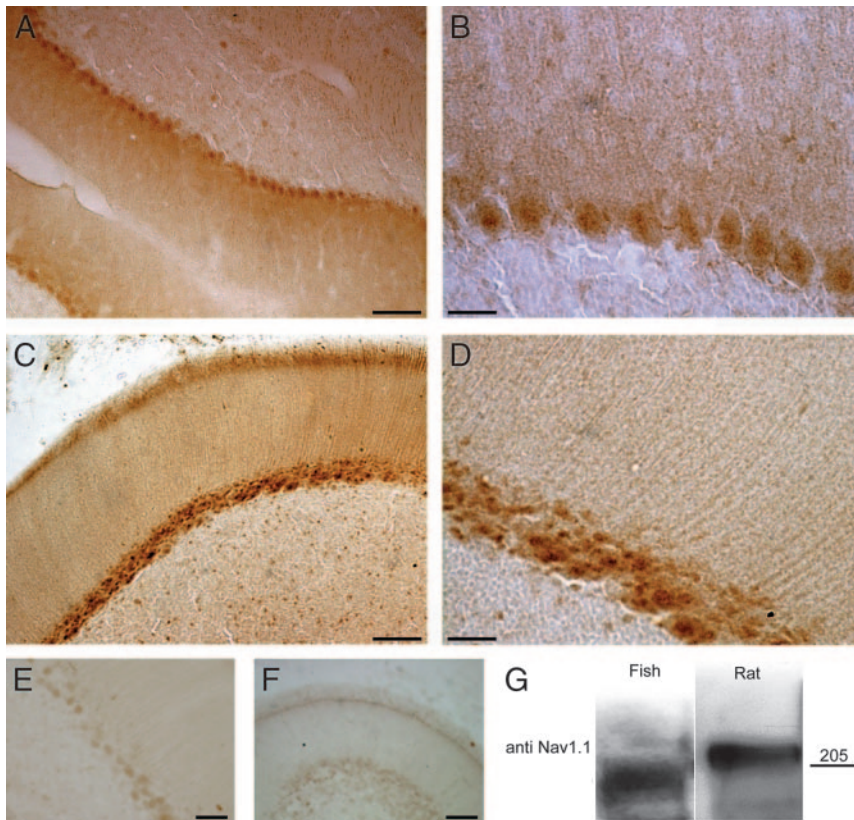


FIG. 3. Na_v1.1 channel staining. *A*: anti-Na_v1.1 channel antibody and DAB staining. Note the denser staining of Na_v1.1 channels in the somata of the rat Purkinje cells vs. the weaker staining in the dendrites. *B*: higher magnification of *A*. *C*: anti-Na_v1.1 channel antibody staining of somata in the ganglion cell layer of mormyrid Purkinje cells. Note the comparable staining pattern between *A* and *C*. Also note the staining of cells in the granule cell layer (*bottom right*). *D*: higher magnification of *C*. Scale bars = 25 μm in *A* and *C* and 6 μm in *B* and *D*. *E*: preadsorption control for anti-Na_v1.1 antibody on a mormyrid cerebellar section. *F*: omission of primary antibody shows weak unspecific binding of secondary antibody comparable to that in *E*. Scale bar = 25 μm in *E* and 6 μm in *F*. *G*: Western blot analysis shows that anti-Na_v1.1 antibodies bind to proteins of the appropriate size in both fish and rat brain membrane preparations.

to be not, or only very lightly, expressed in the granule cell layer (Figs. 3, 4, and 5). Panels *E* and *F* of Figs. 3, 4, and 5 show that when the primary antibody directed against the

respective Na⁺ channel was adsorbed to the antigen before incubation (*E*) or omitted (*F*), no, or only very weak, staining could be detected in mormyrid slices compared with panels *C*

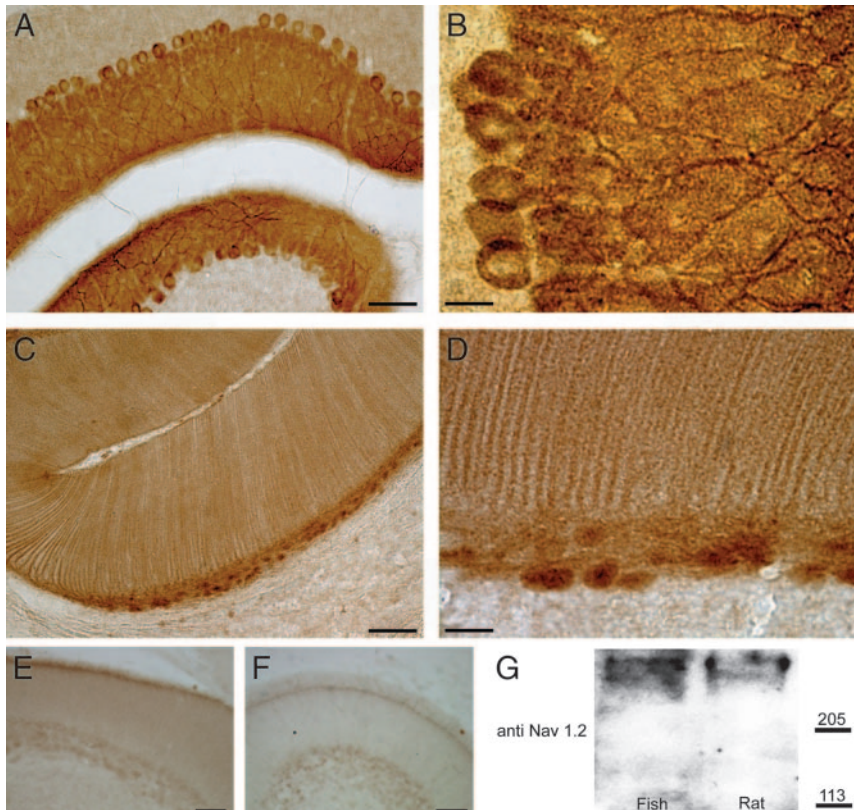


FIG. 4. Na_v1.2 channel staining. *A*: anti-Na_v1.2 channel antibody and DAB staining. Na_v1.2 staining is equally dense in the somata and dendrites of rat Purkinje cells. *B*: higher magnification of *A*. *C*: same staining as in *A* but now of mormyrid Purkinje cells. Note that the density of the Na_v1.2 staining is comparable between rat and fish Purkinje cells. *D*: higher magnification of *C*. Scale bars = 25 μm in *A* and *C* and 6 μm in *B* and *D*. *E*: preadsorption control for anti-Na_v1.2 antibody on a mormyrid cerebellar section. *F*: omission of primary antibody shows weak unspecific binding of secondary antibody comparable to that in *E*. Scale bars = 25 μm in *E* and *F*. *G*: Western blot analysis shows that anti-Na_v1.2 antibodies bind to proteins of the appropriate size in both fish and rat brain membrane preparations.

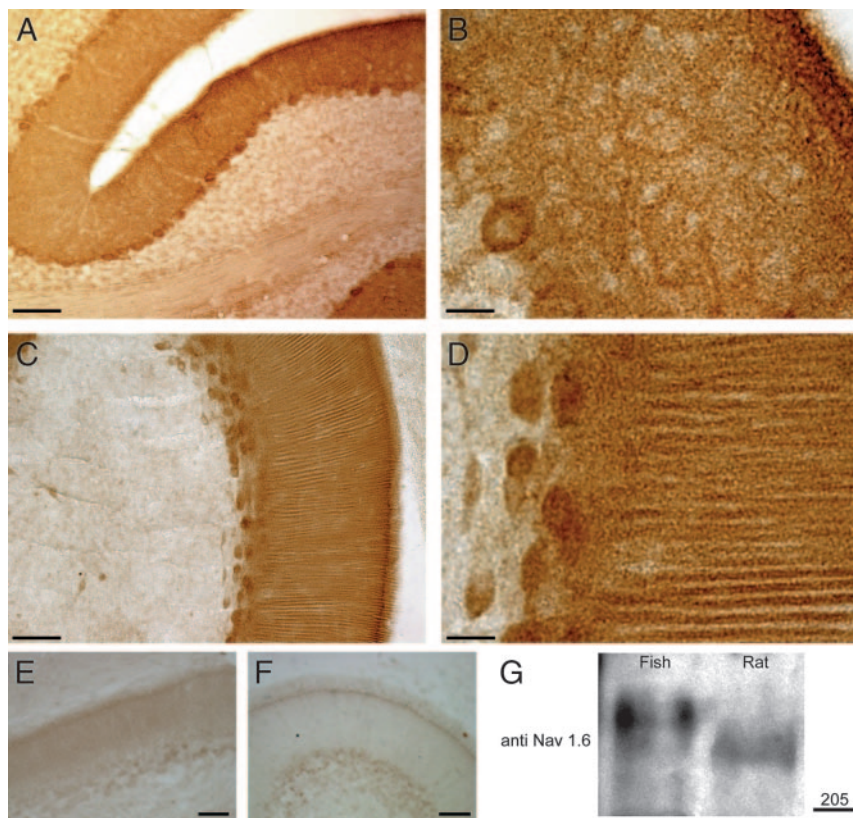


FIG. 5. $\text{Na}_v1.6$ channel staining. *A*: anti- $\text{Na}_v1.6$ channel antibody and DAB staining. $\text{Na}_v1.6$ staining in the rat is present in the somata and in the dendrites. *B*: higher magnification of *A*. *C*: same staining as in *A* but now of mormyrid Purkinje cells. Note that the density of the $\text{Na}_v1.6$ staining is comparable between rat and fish Purkinje cells. *D*: higher magnification of *C*. Scale bars = 25 μm in *A* and *C* and 6 μm in *B* and *D*. *E*: preadsorption control for anti- $\text{Na}_v1.6$ antibody on a mormyrid cerebellar section. *F*: omission of primary antibody shows weak unspecific binding of secondary antibody comparable to that in *E*. Scale bars = 25 μm in *E* and *F*. *G*: Western blot analysis shows that anti- $\text{Na}_v1.6$ antibodies bind to proteins of the appropriate size in both fish and rat brain membrane preparations.

and *D* of Figs. 3, 4, and 5. When we compare panels *E* and *F* we can conclude that the very weak staining that is still found after adsorption and omission of the antibody can be fully attributed to weak unspecific staining of the secondary antibody used. In addition, Western blot analysis (*G* panels of Figs. 3, 4, and 5) shows that antibodies directed against $\text{Na}_v1.1$, $\text{Na}_v1.2$, and $\text{Na}_v1.6$ stain proteins of the expected molecular size in both fish and rat brain membrane preparations. These results show that the Na^+ channel antibodies used in this study are specific for the antigen against which they are directed (*E* panels of Figs. 3, 4, and 5) and that these antibodies react to proteins of the appropriate size in mormyrid fish brain membrane preparations (*G* panels of Figs. 3, 4, and 5). The secondary antibody used does only very weakly stain the cerebellar sections to a degree that does not interfere with the interpretation of our results (*F* panels of Figs. 3, 4, and 5). Purkinje cells of both species express the same subset of Na^+ channels in comparable densities at comparable sites. To examine whether the immunohistochemically characterized Na^+ channels are functional and to compare Na^+ conductances in Purkinje cells of rats and mormyrid fish, we set out to study different types of Na^+ conductances using patch-clamp electrophysiological recordings.

Electrophysiological characterization of Na^+ conductances

We first recorded from dissociated neurons to minimize space-clamp limitations and thus to allow for a characterization of current properties. Voltage steps (20-ms depolarizing step from -90 to $+30$ mV; Fig. 6*A*) resulted in a fast inactivating TTX-sensitive Na^+ current in dissociated rat Purkinje cells ($n = 6$, Fig. 6, *B* and *F*). The displayed traces show the

TTX-sensitive current components after subtraction of the currents that remained when TTX was bath-applied. In the following, the TTX-sensitive currents remaining after subtraction are labeled as "TTX subtracted." In dissociated mormyrid Purkinje cells, we found a similar fast inactivating current ($n = 6$, all TTX subtracted; Fig. 6, *C* and *F*). Sodium currents were corrected for input capacitance [16.6 ± 1.1 pF (\pm SE) for rat ($n = 5$) and 9.8 ± 0.7 pF (\pm SE) for mormyrid ($n = 5$) Purkinje cells] and plotted as current density on a pA/pF scale. This was done to correct for the smaller size of mormyrid Purkinje cell somata. The fast inactivating Na^+ current reached 189 ± 57 pA/pF (\pm SE) with a decay time constant of 0.31 ± 0.049 ms (\pm SE) in rat Purkinje cells ($n = 6$, all TTX subtracted) and 179 ± 59 pA/pF (\pm SE) with a decay time constant of 0.47 ± 0.056 ms (\pm SE) in mormyrid Purkinje cells ($n = 6$, all TTX subtracted, $P > 0.05$, Mann-Whitney *U* test) (Fig. 6, *H* and *L*). Fast inactivating current rise times also did not differ between species [0.38 ± 0.052 ms (\pm SE) for rat and 0.39 ± 0.008 ms (\pm SE) for mormyrid dissociated cells, $P > 0.05$, Mann-Whitney *U* test] (Fig. 6*J*). Our data from rat dissociated Purkinje cells are very similar to those previously obtained from isolated rat Purkinje cell somata (Raman and Bean 1997).

To test for the presence of resurgent Na^+ currents in the dissociated cell preparations, the depolarizing voltage steps were followed by repolarizing steps to potentials between 0 and -60 mV (rat, $n = 6$, all TTX subtracted; fish, $n = 6$, all TTX subtracted) (Fig. 6*A*). Resurgent Na^+ currents were elicited in mormyrid fish and rat Purkinje cells during repolarization steps (Fig. 6, *B*, *C*, and *E*), which were very similar to resurgent Na^+ currents previously described in rat and mouse cerebellar Purkinje cells using the same protocol (Raman and Bean 1997; Raman et al. 1997). In rat Purkinje cells, the

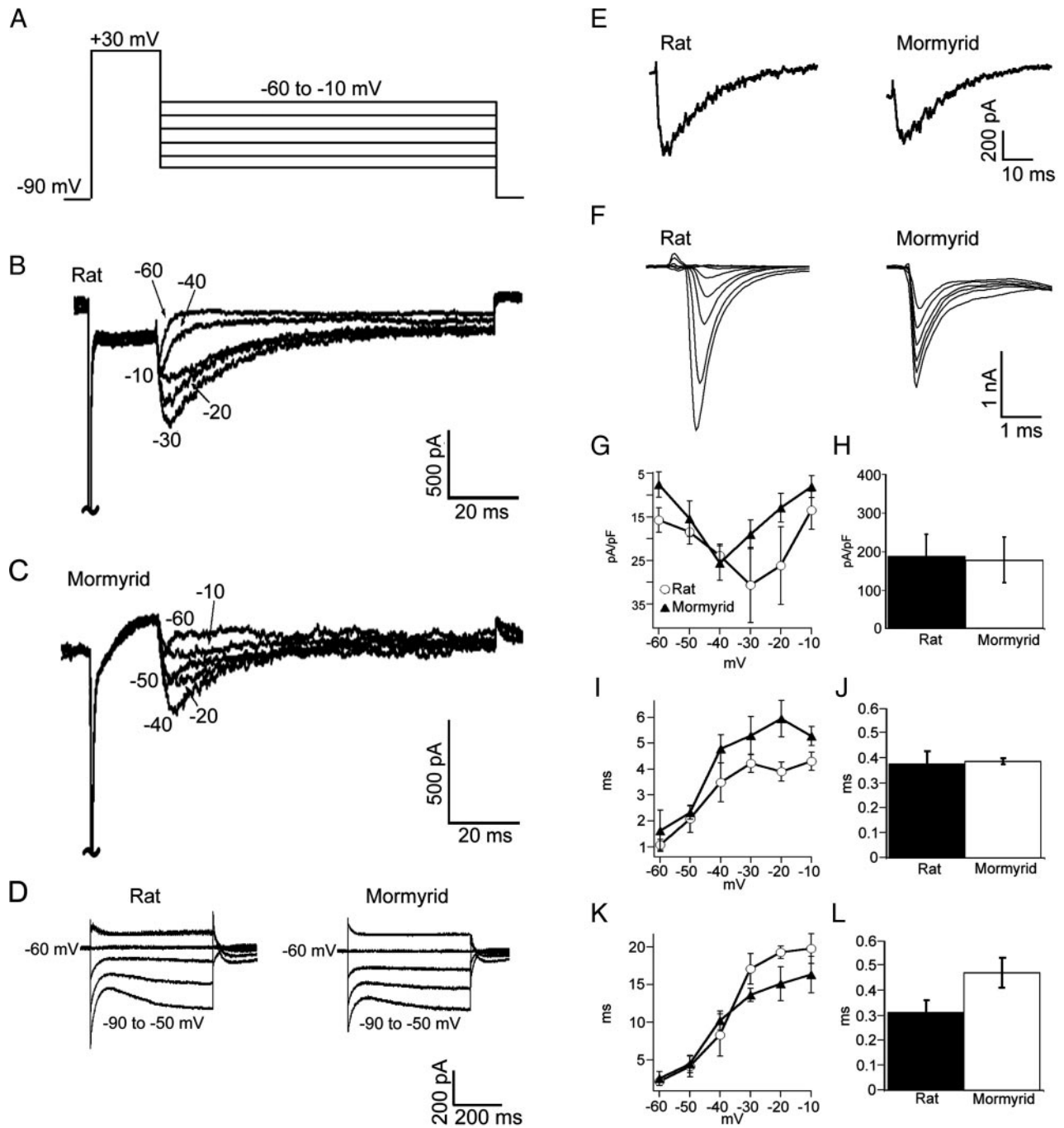


FIG. 6. Fast inactivating and resurgent Na⁺ currents recorded from dissociated rat and mormyrid fish Purkinje neurons. *A*: voltage-step protocol used to elicit Na⁺ currents. *B*: tetrodotoxin (TTX)-subtracted fast inactivating (+30-mV step) and resurgent Na⁺ currents (−60- to −10-mV steps) recorded from rat dissociated Purkinje neurons. *C*: TTX-subtracted fast inactivating and resurgent Na⁺ currents recorded from mormyrid dissociated Purkinje neurons. *D*: voltage-step protocols were applied to determine the input resistances of rat (*left*) and fish (*right*) Purkinje cells. *E*: enlargement of peak resurgent Na⁺ currents recorded. *F*: fast Na⁺ currents recorded during wash-in of TTX. *G*: current–voltage relationship of resurgent Na⁺ currents. *H*: peak fast Na⁺ current. *I*: rise time of resurgent Na⁺ currents. *J*: rise time of fast Na⁺ current. *K*: 50% decay time of resurgent Na⁺ currents, measured from peak to 50% decay of the peak current. *L*: 50% decay time of fast Na⁺ current. *G–L*: average ± SE, rat *n* = 5, mormyrid *n* = 6.

amplitude of the resurgent current was, at peak, 30.6 ± 8.7 pA/pF (±SE) with a rise time of 4.22 ± 0.35 ms (±SE) and a decay time constant of 17.1 ± 2.01 ms (±SE) (*n* = 6, all TTX subtracted, step protocol, −30 mV) (Fig. 6, *G*, *I*, and *K*). In mormyrid Purkinje cells, the resurgent Na⁺ current reached 25.6 ± 4.0 pA/pF (±SE) with a rise time of 4.77 ± 0.54 ms (±SE) and a decay time constant of 10.24 ± 1.29 ms (±SE)

(*n* = 6, all TTX subtracted, step protocol, −40 mV) (Fig. 6, *G*, *I*, and *K*). Resurgent current peak size and rise and decay times were all not significantly different between rat and mormyrid Purkinje cells at all voltage steps (*P* > 0.05, Mann–Whitney *U* test). There was also no difference in the input resistance (rats, *n* = 5: 104.9 ± 13.1 MΩ; fish, *n* = 4: 97.1 ± 13.3 MΩ; *P* > 0.05; Mann–Whitney *U* test; Fig. 6*D*). Our observations sug-

gest that the types of conductances described here are of somatic origin. This assumption is supported by the immunohistochemical data. A caveat, however, is that the dissociated Purkinje cells often still contain axon and dendrite stumps. Therefore it is not possible to exclude contributions from these structures to the recorded conductances.

Although recordings from dissociated neurons provide the best technical approach to characterize Na^+ currents, they are limited by difficulties in distinguishing different types of neurons. This aspect is particularly relevant for the mormyrid cerebellum because here Purkinje cells and efferent cells are quite similar and are, in fact, indistinguishable after dissociation. Therefore we performed an additional series of recordings from Purkinje cells in slices to qualitatively confirm the observations described above. Purkinje cells were identified by the superficial position of their somata in the ganglion cell layer (Meek and Nieuwenhuys 1991). Voltage steps (20-ms depolarizing step from -90 to $+30$ mV; Fig. 7A) resulted in a fast inactivating TTX-sensitive Na^+ current in rat Purkinje cells ($n = 15$, of which three were TTX subtracted; Fig. 7B). Sodium currents were corrected for input capacitance [$1,013 \pm 195$ pF (\pm SE) for rat ($n = 5$) and 833 ± 92 pF (\pm SE) for mormyrid ($n = 5$) Purkinje cells] and plotted on a pA/nF scale. The fast current component was followed by a slower, low-

amplitude current. In mormyrid Purkinje cells, we found a similar biphasic current ($n = 10$, of which five were TTX subtracted; Fig. 7D). The fast inactivating Na^+ current differed in amplitude ($P < 0.05$, Mann-Whitney U test), but not in rise or decay time constant ($P > 0.05$, Mann-Whitney U test, measured at 50% decay) between the two species, even after compensation for cell capacitance. This difference might be a result of the poor space-clamp conditions in intact Purkinje cells, which makes a good estimate of cell capacitance virtually impossible. The current reached 3.78 ± 0.71 nA/nF (\pm SE) with a decay time constant of 0.80 ± 0.19 ms (\pm SE) in rat Purkinje cells ($n = 3$, all TTX subtracted) and 1.31 ± 0.62 nA/nF (\pm SE) with a decay time constant of 1.02 ± 0.24 ms (\pm SE) in mormyrid Purkinje cells ($n = 6$, all TTX subtracted) (Fig. 7, F and G). Rise times were 0.42 ± 0.066 ms (\pm SE) in rats and 0.37 ± 0.048 ms (\pm SE) in mormyrids (Fig. 7G).

Because these recordings were obtained from intact Purkinje cells and not from isolated somata, it is possible that inadequate space clamp in some cells allowed for voltage escape during the depolarizing step (for a discussion of the space-clamp problem see Häusser 2003). Despite this technical limitation that makes a reliable quantification difficult to achieve, these data from intact slices are similar to those obtained in our dissociated cell experiments and to those previously obtained

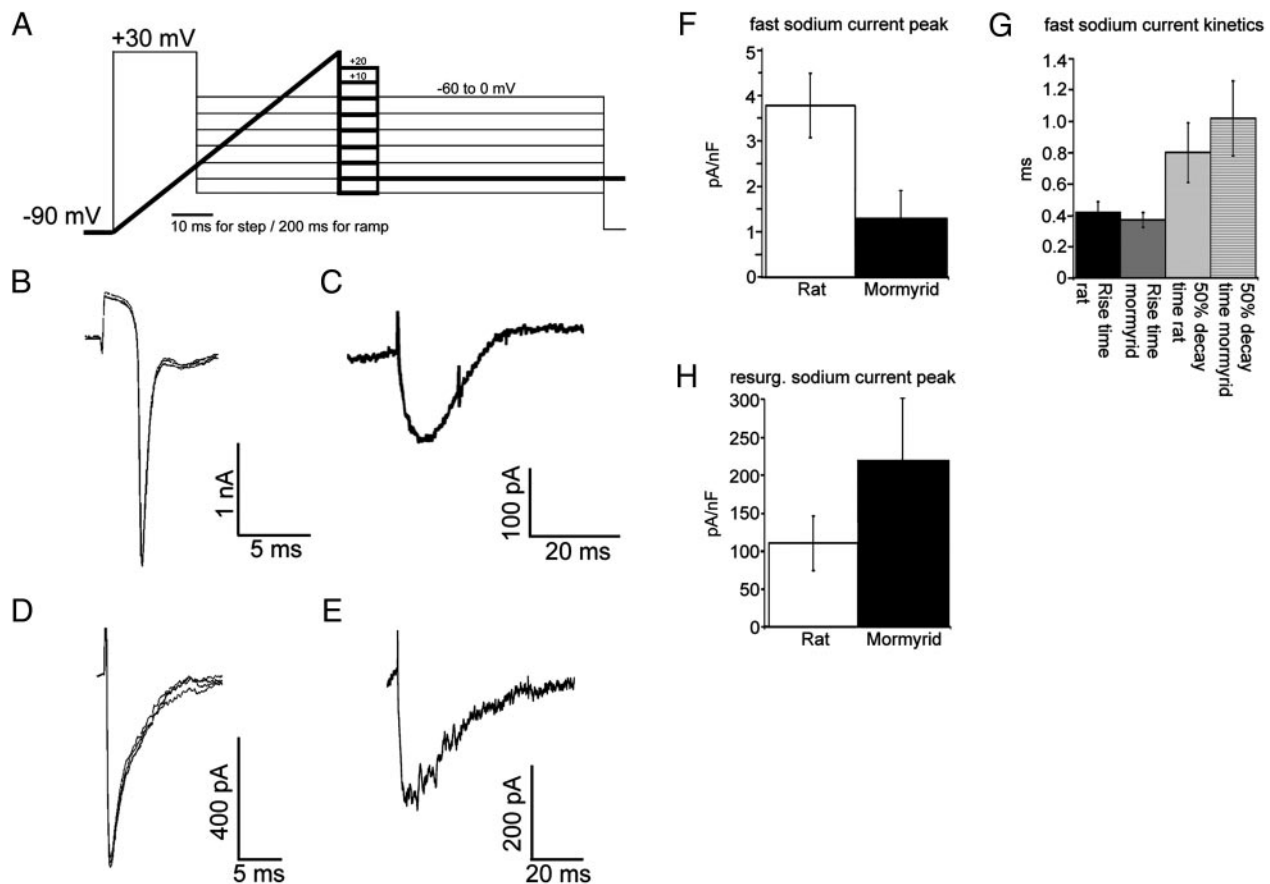


FIG. 7. Fast inactivating and resurgent Na^+ currents recorded from rat and mormyrid fish cerebellar Purkinje neurons in slices. A: voltage-step and voltage-ramp protocols used to elicit Na^+ currents. Note the different timescales. B: 3 consecutive TTX-subtracted fast Na^+ current traces recorded 20 s apart during voltage steps from -90 to $+30$ mV from a rat Purkinje cell. C: TTX-subtracted resurgent Na^+ current recorded from a rat Purkinje cell during a step from $+30$ to -30 mV. D: same as in B but from mormyrid Purkinje cell. E: same as in C but from mormyrid Purkinje cell. F: peak fast Na^+ current recorded from rat (average \pm SE, $n = 3$) and mormyrid (average \pm SE, $n = 5$) Purkinje cells in slices. G: fast Na^+ current kinetics recorded from rat (average \pm SE, $n = 3$) and mormyrid (average \pm SE, $n = 5$) Purkinje cells in slices. H: peak resurgent Na^+ current recorded from rat (average \pm SE, $n = 7$) and mormyrid (average \pm SE, $n = 6$) Purkinje cells in slices.

from isolated rat Purkinje cell somata (Raman and Bean 1997). Furthermore they strongly resemble fast current recordings recently obtained from intact Purkinje cells in slices (Afshari et al. 2004). An interesting side note is that after dissociation, the input capacitance decreases to a comparably larger degree than the Na⁺ current amplitudes (in both rat and mormyrid Purkinje cells), providing further evidence that the Na⁺ channel density is particularly high in the soma (see also distribution of Na_v1.1 channels in Fig. 3). To test for the presence of resurgent Na⁺ currents, the depolarizing voltage steps were followed by repolarizing steps to potentials between 0 and -60 mV [rat (*n* = 15) of which three were TTX subtracted; fish (*n* = 10), five TTX subtracted] (Fig. 7A). Alternatively, we used ramp protocols [0.1 mV/ms from -90 to +30 mV followed by repolarizing steps between +20 and -60 mV; fish (*n* = 6), rat (*n* = 7); all TTX subtracted; Fig. 7, C, E, and H). Both protocols elicited resurgent Na⁺ currents in mormyrid fish and rat Purkinje cells during repolarization (Fig. 7, C and E), which were resembling the resurgent Na⁺ currents we recorded in dissociated cells and those previously described in rat and mouse dissociated cerebellar Purkinje cells using the same protocol (Raman and Bean 1997; Raman et al. 1997). The resemblance between our slice data and previously published work on slices (Afshari et al. 2004) is again striking. In rat Purkinje cells, the amplitude of the resurgent current was 110.32 ± 36.19 pA/nF (\pm SE) (*n* = 4, all TTX subtracted, ramp protocol, -30 mV) (Fig. 7H). In mormyrid Purkinje cells, the resurgent Na⁺ current reached 219.30 ± 82.33 pA/nF (\pm SE) (*n* = 4, all TTX subtracted, ramp protocol, -30 mV) (Fig. 7H) (*P* > 0.05, Mann-Whitney *U* test). No attempt was made to quantify the voltage dependency, or kinetics, of the resurgent currents in slices because the voltage at which the peak amplitude was measured and the kinetics of the resurgent current varied from cell to cell probably because of space-clamp problems. In all recordings, however, the voltage dependency of the resurgent current was clearly seen. There was no difference in the input resistance between rat and mormyrid Purkinje cells in slices (rat: 84.8 ± 18.5 M Ω ; *n* = 5; fish: 81.3 ± 13.1 M Ω ; *n* = 5; *P* > 0.05, Mann-Whitney *U* test; data not shown).

The immunohistochemical and electrophysiological data shown above indicate that rat and mormyrid Purkinje cells qualitatively share the same set of Na⁺ conductances. Nevertheless, CF stimulation does not evoke complex spikes in mormyrid Purkinje cells. Isolated somata of rat Purkinje cells can still fire complex spikes. The underlying Na⁺ currents have been examined in the dynamic-clamp configuration, which allows application of a complex spike as the command potential and recording of isolated currents in voltage-clamp mode. In this configuration, rat Purkinje cells are able to elicit Na⁺ currents at the high frequency that is typical for the spike components of a complex spike (Raman and Bean 1997). It was suggested that this ability to fire conglomerate action potentials arises from resurgent Na⁺ currents, which recover rapidly from inactivation. To test whether the observed differences in CF responses between rat and mormyrid Purkinje cells result from differences in the ability to repetitively activate Na⁺ conductances at the frequency required to fire a complex spike, we applied the dynamic-clamp technique to dissociated rat and mormyrid Purkinje cells (Fig. 8). The complex spike used as a command potential was recorded from an intact

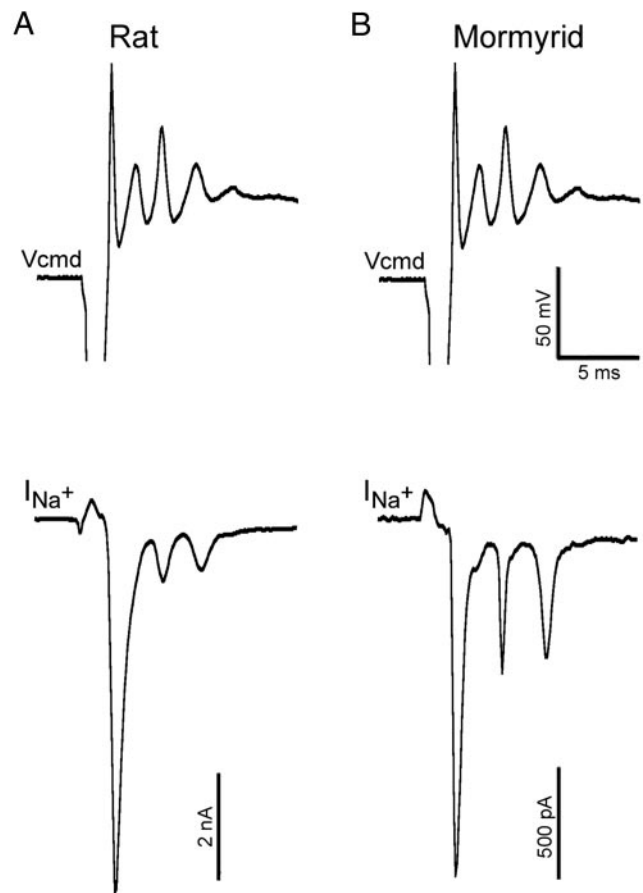


FIG. 8. Na⁺ currents recorded in dynamic-clamp configuration in response to a complex spike applied as a command potential. *A*, top trace: command waveform that was applied to a dissociated rat Purkinje cell. Complex spike was recorded in a cerebellar slice from an intact Purkinje cell in current-clamp mode. Bottom trace: Na⁺ current (TTX subtracted) recorded from a dissociated Purkinje cell in voltage-clamp mode. *B*: same command waveform was applied to a dissociated mormyrid Purkinje cell in voltage-clamp mode. Bottom trace: Na⁺ current (TTX subtracted). Note the different current amplitude scale in *B*.

Purkinje cell in a rat cerebellar slice. Dissociated Purkinje cells from both rats (Fig. 8A; *n* = 7; four TTX subtracted) and mormyrid fish (Fig. 8B; *n* = 7; three TTX subtracted) were able to respond to the spike components with transient Na⁺ currents. A notable exception in both rat and fish Purkinje cells was the first small spikelet of the complex spike waveform. This first spikelet did not elicit a separate current transient (Fig. 8, A and B). Such failure was not observed by Raman and Bean (1997), but it should be noted that the frequency of spike components in the command potential applied here was higher, which could explain the current transient failure, particularly after the large initial transient. It is obvious from the traces shown in Fig. 8 that the initial Na⁺ current recorded from the rat Purkinje cell is larger than that recorded from the mormyrid Purkinje cell, although in both recordings the same command potential was applied. However, the absence of qualitative differences in the command potential-evoked currents between rat and mormyrid Purkinje cells shows that the somata of mormyrid Purkinje cells possess the Na⁺ conductances required to support repetitive action potential firing as well. Thus our somatic recordings did not reveal any differences in Na⁺

conductances that could provide an explanation for an absence of synaptically evoked complex spikes in mormyrid fish.

DISCUSSION

The dendritic tree architecture of Purkinje cells and their electrophysiological characteristics differ substantially between mormyrid fish and mammals. These differences motivated us to better characterize Purkinje cells of the mormyrid fish *Gnathonemus petersii* using both immunohistochemical and electrophysiological approaches. In this initial study, we focused on Na⁺ currents because the most striking electrophysiological differences are related to Na⁺ spike activity: 1) unusually low Na⁺ spike amplitudes; and 2) the absence of complex spikes, including their fast, initial Na⁺ spike component.

Our immunohistochemical experiments show that the Na⁺ channel α -subunits Na_v1.1, Na_v1.2, and Na_v1.6 are present in comparable densities and locations in the mormyrid and rat cerebellum (Figs. 3, 4, and 5). Na_v1.1 is expressed in Purkinje cell somata, but the staining in the molecular layer is weak and does not allow resolution of dendrites. In mammalian Purkinje cells, Na⁺ action potentials do not backpropagate into the dendrite, which is partially attributed to a low dendritic Na⁺ channel density (Stuart and Häusser 1994). Our observations raise the question whether Na_v1.1 channels need to be present at a certain density to allow action potentials to backpropagate into the dendrites. Of the three types of Na⁺ channel α -subunits, only Na_v1.1 is also expressed in somata in the granule cell layer of both species. In contrast to the Na_v1.1 subunits, Na_v1.2 and Na_v1.6 were found to be densely expressed in somata of both rat and mormyrid Purkinje cells as well as in the molecular layer. We cannot rule out the possibility that the staining in the molecular layer reflects the expression of these Na⁺ channel α -subunits in PF terminals. Staining of these subunits has been described in granule cell ascending axons and parallel fibers (Schaller and Caldwell 2003). In our immunohistochemical experiments, however, we did not see staining of granule cell somata or axons above background levels. The expression of Na_v1.2 in mammalian Purkinje cells has been debated (Black et al. 1994; Felts et al. 1997; but see Brysch et al. 1991; Gong et al. 1999; for review see Schaller and Caldwell 2003). Our data indicate that Na_v1.2 is expressed in somata and dendrites of rat Purkinje cells and thus support the findings of Waxman and colleagues (Black et al. 1994; Felts et al. 1997). Na_v1.6 channels were strongly expressed in somata and dendrites of rat and fish Purkinje cells as well. So far, the resurgent Na⁺ current, which is attributed to Na_v1.6 channels, has been described on the basis of somatic patch-clamp recordings (Raman and Bean 1997, 2001). Our data suggest that this current exists in the dendrites as well.

Next, we conducted voltage-clamp experiments to investigate whether the Na⁺ channels found to be expressed in the mormyrid cerebellum could mediate the same set of voltage-gated conductances as the Na⁺ channels expressed in rat Purkinje cells. The present results show that a depolarizing voltage step activates a TTX-sensitive, fast inactivating Na⁺ current in dissociated Purkinje cells of both rats and mormyrid fish, which is followed by a low-amplitude tail component in slice recordings. Although the fast inactivating current was clearly present in both preparations, it reached higher ampli-

tudes in rat than in mormyrid Purkinje cells in slices. Using a voltage-step (dissociated cells and slices) or a ramp (slices only) protocol, we could demonstrate a TTX-sensitive resurgent Na⁺ current in both rats and fish, which strongly resembled the resurgent Na⁺ current described earlier (Afshari et al. 2004; Raman and Bean 1997). The resurgent currents had indistinguishable amplitudes in rat dissociated cells compared with mormyrid cells after capacitance compensation ($P > 0.05$, Mann-Whitney U rank test) and these amplitudes were well within the range of data published earlier (Afshari et al. 2004; Raman and Bean 1997). Rise and decay time constant ranges in the two species were overlapping and were also similar to previously published data (Afshari et al. 2004; Raman and Bean 1997). The recordings in slices were added to demonstrate that the resurgent currents are indeed present in Purkinje cells (because they cannot be distinguished with certainty from similar cells once being dissociated) under more physiological conditions (without their dendrites being cut). Resurgent Na⁺ currents have so far been described in only a limited number of different types of neurons. In the cerebellum, they were described in Purkinje cells (Raman and Bean 1997), unipolar brush cells (Afshari et al. 2004; Mossadeghi and Slater 1998), deep cerebellar nuclei cells (Afshari et al. 2004), and granule cells (Afshari et al. 2004; D'Angelo et al. 2001). Our results show that mormyrid Purkinje cells, which otherwise differ in several morphological and physiological parameters from their mammalian counterparts, can be added to the list.

We have performed all immunohistochemical and electrophysiological experiments in slices or dissociated neurons from both rats and mormyrid fish to allow for a direct comparison. Although there are obvious differences in electrophysiological response characteristics, we did not detect differences in the expression pattern of Na_v1.1, Na_v1.2, or Na_v1.6 subunits, or in fast inactivating or resurgent Na⁺ currents. Moreover, the dynamic-clamp recordings shown in Fig. 8 indicate that dissociated rat and mormyrid Purkinje cells (which basically consist of isolated somata) respond to a complex spike applied as the command potential with repetitive Na⁺ current transients. Thus rat and mormyrid Purkinje cells also show no differences in their ability to activate Na⁺ conductances at high enough frequencies to support complex spike firing. Although these observations allow us to conclude that the different electrophysiologies do not arise from differences in the functional expression pattern of these three types of Na channel α -subunits, they do not allow any conclusion with respect to what other parameters are causing these differences instead. Possible candidates are differences in the expression pattern of voltage-gated K⁺ or Ca²⁺ channels or the different dendrite morphologies (see also Mainen and Sejnowski 1996; Vetter et al. 2001).

Two types of electrophysiological differences were of particular interest to us: the absence of complex spikes in mormyrid Purkinje cells and their low-amplitude Na⁺ spikes. The complex spike received attention after recent demonstrations of synaptic plasticity at the CF synapses, involving long-term changes of slow complex spike components (Hansel and Linden 2000; Hansel et al. 2001; Weber et al. 2003). These results stimulated some interest in the ionic composition of the slow complex spike components (for a discussion see Schmolesky et al. 2002). It has been suggested that resurgent Na⁺ currents might be characteristic for types of rapidly firing

neurons (Afshari et al. 2004) and might allow Purkinje cells to generate the high-frequency spikelets that make up the late complex spike components (Raman et al. 1997; Schmolesky et al. 2002). Our results show that, whereas mormyrid Purkinje cells do not fire complex spikes, they still show resurgent Na⁺ currents. What other parameters might then cause the absence of complex spikes in mormyrid Purkinje cells? As we argued above, the unique dendrite morphology might be involved, but at this point we simply do not understand the impact of this parameter on spike patterns well enough to argue what specific features of mormyrid Purkinje cell dendrites would prevent complex spike firing. Moreover, burst firing (as in complex spikes) can also be evoked in dissociated Purkinje cells (Swensen and Bean 2003). This observation does not exclude an impact of the dendrite morphology on the occurrence or waveform of complex spikes, but it shows that this characteristic all-or-none response of mammalian Purkinje cells can be evoked in isolated somata.

To examine whether isolated somata of mormyrid Purkinje cells share this ability to support complex spike firing, we used the dynamic-clamp technique to apply complex spikes as command potentials to dissociated rat and mormyrid Purkinje cells (Fig. 8). Remarkably, the ability to activate Na⁺ current transients in response to individual spikelets present in the complex spike waveform can also be found in mormyrid Purkinje cells. This observation indicates that there are no qualitative differences in electrophysiological parameters between isolated somata of rat and mormyrid Purkinje cells. These findings add weight to the hypothesis that the absence of synaptically evoked complex spikes in mormyrid Purkinje cells arises from synaptic/dendritic integration properties, which might be based on morphological differences. However, no direct evidence is available yet to support this idea and thus other factors need to be considered as well. For example, differences in response amplitudes could have an impact on response characteristics. The observed difference in the CF-EPSC amplitude (Fig. 1D) could, for example, play a role in the different response patterns. Our recordings of CF responses of different amplitudes and at different membrane potentials allow us, however, to exclude the possibility that this phenomenon is solely related to the spike threshold. Remarkably, a larger amplitude was also observed when comparing the fast inactivating Na⁺ current measured in rat Purkinje cells in slices to those recorded in fish Purkinje cells (Fig. 7). A similar amplitude difference in the initial spike component can be seen in the dynamic-clamp recording shown in Fig. 8. The hypothesis that a lower Na⁺ current amplitude explains the absence of complex spikes in fish Purkinje cells, however, is not supported by the data that are best suited for a quantitative comparison: we did not detect either significant differences in the amplitudes of the fast inactivating Na⁺ current or the resurgent Na⁺ current in dissociated Purkinje cells (Fig. 6).

Interestingly, the initial complex spike component, attributed to a somatic Na⁺ spike, is completely absent in mormyrid Purkinje cells. Na⁺ spikes can be recorded in these neurons, but they do not reach the amplitudes seen in other types of neurons and typically stay below 30 mV. As outlined above, we could not detect significant differences in Na⁺ current amplitudes in the dissociated cell configuration. Therefore we consider it more likely that the difference in Na⁺ spike amplitudes has morphological causes. For example, the thin, unmy-

elinated axons of mormyrid Purkinje cells might reduce axonal spike propagation from the axonal spike initiation zone, which has been shown in rat Purkinje cells to be at the first node of Ranvier (Clark et al. 2005), toward the soma (see also Han and Bell 2003).

Purkinje cells of mormyrid fish are very interesting for reasons that go beyond the described differences in synaptic responses and in Na⁺ spike activity. They are, for example, optimally suited to study the impact of dendritic tree architecture (e.g., degree of dendritic branching) on dendritic integration and spike propagation (see Vetter et al. 2001). Further studies on the expression profiles of voltage-dependent ion channels will be necessary to better understand what electrophysiological or morphological parameters critically contribute to the unique response features of mormyrid Purkinje cells.

ACKNOWLEDGMENTS

We are grateful to P. French, E. D. Haasdijk, A. Vlugs, and E. Teuling for excellent technical assistance and we thank Drs. C. C. Bell, V. Z. Han, and D. Jaarsma for helpful discussions and comments on the manuscript.

GRANTS

This work was supported by Netherlands Organization for Scientific Research Grants NWO-MW 903.47.190 to C. I. De Zeeuw and NWO-ALW 812.07.006 to C. Hansel and a Royal Dutch Academy of Sciences grant to C. Hansel.

REFERENCES

- Afshari FS, Ptak P, Khaliq ZM, Grieco TM, Slater NT, McCrimmon DR, and Raman IM. Resurgent Na currents in four classes of neurons of the cerebellum. *J Neurophysiol* 92: 2831–2883, 2004.
- Bell CC, Caputi A, and Grant K. Physiology and plasticity of morphologically identified cells in the mormyrid electrosensory lobe. *J Neurosci* 17: 6409–6423, 1997b.
- Bell CC, Han VZ, Sugawara Y, and Grant K. Synaptic plasticity in a cerebellum-like structure depends on temporal order. *Nature* 387: 278–281, 1997a.
- Black JA, Yokoyama S, Higashida H, Ransom BR, and Waxman SG. Sodium channel mRNAs I, II and III in the CNS: cell-specific expression. *Brain Res Mol Brain Res* 22: 275–289, 1994.
- Brysch W, Creutzfeldt OD, Luno K, Schlingensiepen R, and Schlingensiepen KH. Regional and temporal expression of sodium channel messenger RNAs in the brain during development. *Exp Brain Res* 86: 562–567, 1991.
- Callaway JC and Ross WN. Spatial distribution of synaptically activated sodium concentration changes in cerebellar Purkinje neurons. *J Neurophysiol* 77: 145–152, 1997.
- Clark BA, Monsivais P, Branco T, London M, and Häusser M. The site of action potential initiation in cerebellar Purkinje neurons. *Nat Neurosci* 8: 137–139, 2005.
- D'Angelo E, Nieuws T, Maffei A, Armano S, Rossi P, Taglietti V, Fontana A, and Naldi G. Theta-frequency bursting and resonance in cerebellar granule cells: experimental evidence and modeling of a slow K⁺-dependent mechanism. *J Neurosci* 21: 759–770, 2001.
- Do MT and Bean BP. Sodium currents in subthalamic nucleus neurons from Na_v1.6-null mice. *J Neurophysiol* 92: 726–733, 2004.
- Felts PA, Yokoyama S, Dib-Hajj S, Black JA, and Waxman SG. Sodium channel alpha subunit mRNAs I, II, III, NaG, Na6 and hNE (PN1): different expression patterns in developing rat nervous system. *Brain Res Mol Brain Res* 45: 71–82, 1997.
- Gähwiler BH and Llano I. Sodium and potassium conductances in somatic membranes of rat Purkinje cells from organotypic cerebellar cultures. *J Physiol* 417: 105–122, 1989.
- Garcia KD, Sprunger LK, Meisler MH, and Beam KG. The sodium channel Scn8a is the major contributor to the postnatal developmental increase of sodium current density in spinal motoneurons. *J Neurosci* 18: 5234–5239, 1998.
- Gong B, Rhodes KJ, Bekele-Arcuri Z, and Trimmer JS. Type I and type II Na(+) channel alpha-subunit polypeptides exhibit distinct spatial and tem-

- poral patterning, and association with auxiliary subunits in rat brain. *J Comp Neurol* 412: 342–352, 1999.
- Grieco TM, Afshari FS, and Raman IM.** A role for phosphorylation in the maintenance of resurgent sodium current in cerebellar Purkinje neurons. *J Neurosci* 22: 3100–3107, 2002.
- Grieco TM and Raman IM.** Production of resurgent current in $\text{Na}_v1.6$ -null Purkinje neurons by slowing sodium channel inactivation with β -pompilidotoxin. *J Neurosci* 24: 35–42, 2004.
- Groenewegen HJ and Voogd J.** The parasagittal zonation within the olivocerebellar projection. I. Climbing fiber distribution in the vermis of cat cerebellum. *J Comp Neurol* 174: 417–488, 1977.
- Han VZ and Bell CC.** Physiology of cells in the central lobes of the mormyrid cerebellum. *J Neurosci* 23: 11147–11157, 2003.
- Han VZ, Grant K, and Bell CC.** Reversible associative depression and nonassociative potentiation at a parallel fiber synapse. *Neuron* 27: 611–622, 2000.
- Hansel C and Linden DJ.** Long-term depression of the cerebellar climbing fiber Purkinje neuron synapse. *Neuron* 26: 473–482, 2000.
- Hansel C, Linden DJ, and D'Angelo E.** Beyond parallel fiber LTD: the diversity of synaptic and non-synaptic plasticity in the cerebellum. *Nat Neurosci* 4: 467–475, 2001.
- Häusser M.** Revealing the properties of dendritic voltage-gated channels: a new approach to the space clamp problem. *Biophys J* 84: 3497–3498, 2003.
- Isom LL, Ragsdale DS, De Jongh KS, Westenbroek RE, Reber BF, Scheuer T, and Catterall WA.** Structure and function of the beta 2 subunit of brain sodium channels, a transmembrane glycoprotein with a CAM motif. *Cell* 83: 433–442, 1995a.
- Isom LL, Scheuer T, Brownstein AB, Ragsdale DS, Murphy BJ, and Catterall WA.** Functional co-expression of the beta 1 and type IIA alpha subunits of sodium channels in a mammalian cell line. *J Biol Chem* 270: 3306–3312, 1995b.
- Kay AR, Sugimori M, and Llinas R.** Kinetic and stochastic properties of a persistent sodium current in mature guinea pig cerebellar Purkinje cells. *J Neurophysiol* 80: 1167–1179, 1998.
- Khaliq ZM, Gouwens NW, and Raman IM.** The contribution of resurgent sodium current to high-frequency firing in Purkinje neurons: an experimental and modeling study. *J Neurosci* 23: 4899–4912, 2003.
- Koulen P, Janowitz T, Johnston LD, and Ehrlich BE.** Conservation of localization patterns of IP(3) receptor type 1 in cerebellar Purkinje cells across vertebrate species. *J Neurosci Res* 61: 493–499, 2000.
- Llinas R and Sugimori M.** Electrophysiological properties of in vitro Purkinje cell somata in mammalian cerebellar slices. *J Physiol* 305: 171–195, 1980a.
- Llinas R and Sugimori M.** Electrophysiological properties of in vitro Purkinje cell dendrites in mammalian cerebellar slices. *J Physiol* 305: 197–213, 1980b.
- Mainen ZF and Sejnowski TJ.** Influence of dendritic structure on firing pattern in model neocortical neurons. *Nature* 382: 363–366, 1996.
- Meek J.** Comparative aspects of cerebellar organization. *Eur J Morphol* 30: 37–51, 1992.
- Meek J and Nieuwenhuys R.** Palisade pattern of mormyrid Purkinje cells: a correlated light and electron microscopic study. *J Comp Neurol* 306: 156–192, 1991.
- Mossadeghi B and Slater NT.** Persistent and resurgent sodium currents in cerebellar unipolar brush cells. *Soc Neurosci Abstr* 24: 1078, 1998.
- Nieuwenhuys R and Nicholson C.** Cerebellum of mormyrids. *Nature* 215: 764–765, 1967.
- Nieuwenhuys R and Nicholson C.** Aspects of the histology of the cerebellum of mormyrid fishes. In: *Neurobiology of Cerebellar Evolution and Development*, edited by Llinas R. Chicago, IL: American Medical Association Education and Research Foundation, 1969, p. 135–169.
- Pan F and Beam KG.** The absence of resurgent sodium currents in mouse spinal neurons. *Brain Res* 849: 162–168, 1999.
- Raman IM and Bean BP.** Resurgent sodium current and action potential formation in dissociated cerebellar Purkinje neurons. *J Neurosci* 17: 4517–4526, 1997.
- Raman IM and Bean BP.** Inactivation and recovery of sodium currents in cerebellar Purkinje neurons: evidence for two mechanisms. *Biophys J* 80: 729–737, 2001.
- Raman IM, Sprunger LK, Meisler MH, and Bean BP.** Altered subthreshold sodium currents and disrupted firing patterns in Purkinje neurons of *Scn8a* mutant mice. *Neuron* 19: 881–891, 1997.
- Renganathan M, Gelderblom M, Black JA, and Waxman SG.** Expression of $\text{Na}_v1.8$ sodium channels perturbs the firing patterns of cerebellar Purkinje cells. *Brain Res* 959: 235–242, 2003.
- Saper CB and Sawchenko PE.** Magic peptides, magic antibodies: guidelines for appropriate controls for immunohistochemistry. *J Comp Neurol* 465: 161–163, 2003.
- Schaller KL and Caldwell JH.** Expression and distribution of voltage-gated sodium channels in the cerebellum. *Cerebellum* 2: 2–9, 2003.
- Schmolesky MT, Weber JT, De Zeeuw CI, and Hansel C.** The making of a complex spike: ionic composition and plasticity. *Ann NY Acad Sci* 978: 359–390, 2002.
- Sharp AH, Nucifora FC Jr, Blondel O, Sheppard CA, Zhang C, Snyder SH, Russell JT, Ryugo DK, and Ross CA.** Differential cellular expression of isoforms of inositol 1,4,5-triphosphate receptors in neurons and glia in brain. *J Comp Neurol* 406: 207–220, 1999.
- Stuart G and Häusser M.** Initiation and spread of sodium action potentials in cerebellar Purkinje cells. *Neuron* 13: 703–712, 1994.
- Swensen AM and Bean BP.** Ionic mechanisms of burst firing in dissociated Purkinje neurons. *J Neurosci* 23: 9650–9663, 2003.
- Vega-Saenz De Miera E, Rudy B, Sugimori M, and Llinas R.** Molecular characterization of the sodium channel subunits expressed in mammalian cerebellar Purkinje cells. *Proc Natl Acad Sci USA* 94: 7059–7064, 1997.
- Vetter P, Roth A, and Häusser M.** Propagation of action potentials in dendrites depends on dendritic morphology. *J Neurophysiol* 85: 926–937, 2001.
- Weber JT, De Zeeuw CI, Linden DJ, and Hansel C.** Long-term depression of climbing fiber-evoked calcium transients in Purkinje cell dendrites. *Proc Natl Acad Sci USA* 100: 2878–2883, 2003.
- Westenbroek RE, Merrick DK, and Catterall WA.** Differential subcellular localization of the RI and RII Na channel subtypes in central neurons. *Neuron* 3: 695–704, 1989.
- Zenisek D, Henry D, Studholme K, Yazulla S, and Matthews G.** Voltage dependent sodium channels are expressed in nonspiking retinal bipolar neurons. *J Neurosci* 21: 4543–4550, 2001.